Am J Transl Res 2021;13(5):4026-4039
www.ajtr.org /ISSN:1943-8141/AJTR0126163

Original Article

The construction of multifunctional nanoparticles system for dual-modal imaging and arteriosclerosis targeted therapy

Pengda Qiu, Yunhong Xu

Department of Cardiology, The Third Affiliated Hospital of Guangzhou Medical University, No. 63, Duobao Road, Liwan District, Guangzhou 510150, Guangdong, P. R. China

Received November 12, 2020; Accepted March 14, 2021; Epub May 15, 2021; Published May 30, 2021

Abstract: Atherosclerosis is a major risk factor for the development of cardiovascular disease. Unfortunately, due to relatively low sensitivities and poor resolution, the results of surgical resection are often largely unsatisfactory. Moreover, many chemotherapeutic agents, such as curcumin (Cur), are restricted by the low blood-brain barrier (BBB) permeability. Recently, nanotechnology proposes new opportunities to overcome these treatment barriers. In this study, superparamagnetic iron oxide nanoparticles (SPIO) was prepared by the high-temperature solid-state method, and then loaded into amphiphilic polymer DSPE-PEG to form SDP nanoparticles by hydrogen bonding in oil phase. The curcumin was encapsulated in SDP nanoparticles by self-assembly. Finally, vascular cell adhesion molecule-1 (VCAM-1) and Cy5.5 were conjugated on into SDP/Cur nanoparticles by amidation reaction. The average particle size of the prepared multifunctional SDP-VCAM-1/Cur/Cy5.5 nanoparticles is 124.4 nm, which can provide the sustained release of Cur. Moreover, the nanoparticles are proved to have superparamagnetic properties and fluorescence properties. *In vitro* cell experiments show that nanoparticles have excellent biocompatibility, blood compatibility and macrophage targeting. These results show that SDP-VCAM-1/Cur/Cy5.5 nanoparticles can be used not only as dual imaging probe for magnetic resonance (MR) and fluorescence imaging, but also as carriers to deliver chemotherapeutic drugs to inflammatory tissue, thus providing a promising opportunity for the treatment, molecular imaging and targeted therapy in atherosclerosis due to their established specificity and safety.

Keywords: SPIO NPs, MRI, fluorescence imaging, VCAM-1, atherosclerosis

Introduction

With the development of society and the increase of life pressure, cardiovascular disorder has gradually become the most important factor threatening human health, in which atherosclerosis had extremely severe destructive [1, 2]. Atherosclerosis can cause local vascular lesions, which can lead to a series of complications, such as stroke, thrombus and even threaten our life [3]. In the early process of plaque formation, if the lesion area can be well diagnosed and treated, it can effectively reduce the damage of atherosclerosis to human beings [4]. Although certain therapeutic methods, including stent implantation, have been developed for atherosclerosis treatment, most of the patients are in the mid-late stage of the disease at the time of diagnosis [5, 6]. This is due to the wall thickening and lesion develops to the outside of the wall rather than the lumen in the early stage of the disease [7]. Thus, current diagnosis and treatment exhibit hysteresis. In early phase of plaque formation, the early diagnosis and treatment of atherosclerotic plaques by imaging will contribute to reduce the threat of atherosclerosis to human health.

Among the many imaging methods, magnetic resonance imaging (MRI) has become a powerful imaging technology recognized [8]. The imaging principle is the signal intensity, which is dependent on the relaxation of protons by an external magnetic field [9]. Currently. MRI is classified into different categories based on relaxation properties, i.e., longitudinal relaxation (T1) and transverse relaxation (T_2) [10]. In general, the complex of gadolinium (Gd) is

selected as the contrast agent for T1 imaging, and iron oxide nanoparticles (Fe_3O_4) is often selected for T_2 imaging [11, 12]. The biological toxicity of Fe_3O_4 is much smaller than that of Gd, which has gradually become the mainstream contrast agent [13]. Superparamagnetic iron oxide nanoparticles (SPIONs) are excellent magnetic T_2 imaging contrast agents for medical use [14]. Its high magnetic capacity is mainly focused on two aspects: a) the size ranges of SPIONs is mostly between 10 and 30 nm owing to the strong quantum-confinement effect [15]; b) the surface effect (easy to agglomerate) was caused by particle boundary crystal structure defects [16]. Thus, many investigators generally attach a layer of oleamine or oleic acid on the surface of SPIONs to ensure the stability of SPIONs [17]. However, most of the biological environment is aqueous phase, and this kind of oil-soluble iron oxide often needs further modification before use. The common methods of modification include amphiphilic polymer micelles, bifunctional ligands, multi-dentate polymers, silicon shell coating and so on [18]. Previous studies have shown that when SPIONs are incorporated into DSPE-PEG micelles, SPIO nanoparticles could achieve longer circulation half-life, favorable biocompatibility and better surface modification [19].

However, previous MRI single-mode imaging system is often difficult to distinguish the imaging effect in the area with similar gray level due to the imaging mechanism. This requires that we select the regions that can specifically distinguish the gray levels of similar tissues in the choice of the second imaging mode to make up for the deficiency of MRI imaging [20]. Fluorescence imaging exhibits excellent performance, but it should be combined with the advantages of MRI imaging due to its poor penetration [21]. The preparation of a dual model probe with both MRI imaging and fluorescence imaging function has major research implications. The most commonly used fluorescent dyes for bio imaging are fluorescein, cyanine dyes, phthalocyanine dyes, rhodamine fluorescent dyes and so on [22]. Cyanine dyes are widely used in DNA sequencing, staining DNA, biomolecule labeling, *in vivo* imaging, photodynamic therapy and so on [23]. By conjugating a fluorescent dye to a monoclonal antibody, fluorescence imaging can penetrate several centimeters with near infrared light (NIR, 600 nm to 1000 nm wavelength), which is more suitable for small-animal fluorescence imaging *in vivo*. Among them, Cy5.5-NHS is more commonly used in Cy series cyanine dyes, which can directly connect with small peptides through chemically bind [24]. However, there are several major challenges for Cy5.5 in imaging applications such as the trend of rapid accumulation and degradation in aqueous solution, rapid removal from the body, prone to photo bleaching and lack of targeting [25]. These limitations can be overcome by introducing Cy5.5 into the nanoparticle (NP) delivery system [26]. Recently, a large number of polymer nanoparticles and inorganic nanoparticles have been introduced to solve the inherent problems such as Cy5.5 degradation, rapid blood clearance and *in vivo* imaging [27, 28].

The target molecule is also another important part of the nanoparticle targeting diagnosis system. Prior studies have shown that vascular cell adhesion molecule-1 (VCAM-1) is one of the most obvious signs of early atherosclerotic plaque, which is expressed by endothelial cells that form plaques [29]. The overexpression of VCAM-1 is found in only plaque-forming areas in aorta, and is considered to be a specific biomarker of area of aortic lesion formation [30], which makes targeting specificity the ideal choice for drug carriers to gather in atherosclerotic plaques [31]. VCAM-1 targeting has been used to potentiate the delivery of MRI and SPECT contrast agents for imaging at different formation stages of atherosclerosis plaque [32].

In this report, we synthesized and evaluated novel nanoparticles for the treatment and improvement of atherosclerosis, which integrates dual-modal imaging with MRI/fluorescent imaging and chemotherapy. As shown in **Scheme 1**, SPIO nanoparticles and curcumin (Cur) were coated on DSPE-PEG by double-solvent exchange method to obtain SDP/Cur nanoparticles, and then VCAM-1-targeted peptides and Cy5.5-NHS were grafted on DSPE-PEG by covalent bond to obtain SDP-VCAM-1/Cur/Cy5.5. Both SPIO NPs and Cy5.5 play a dual role in MRI/fluorescence bimodal imaging. The synthesis, size and spherical morphology of the polymer were confirmed by ^{1}H NMR and Fourier transform infrared (FTIR) spectroscopy.

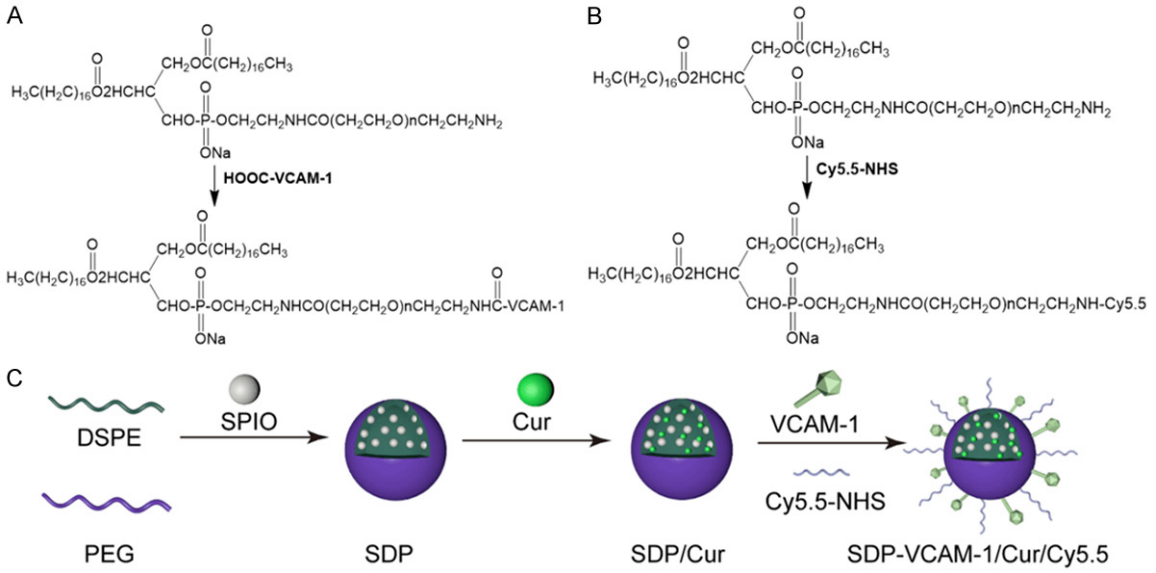

Scheme 1. A. Synthetic route of DSPE-PEG/VCAM-1. B. Synthetic route of DSPE-PEG/Cy5.5. C. Schematic illustration of SDP-VCAM-1/Cur/Cy5.5 nanoassemblies for targeted arteriosclerosis diagnosis and treatment.

The fluorescence properties, magnetic properties and drug loading capacity of the nanoparticles were analyzed by fluorescence spectra, VSM and UV spectra, which has potential biological application. The drug release rate of nanoparticles on atherosclerotic plaque was obtained by simulating the microenvironment of atherosclerotic plaque. Finally, the cytotoxicity of nanoparticles was evaluated via CCK-8 assays and targeting of nanoparticles was demonstrated to the uptake in macrophages.

Material and methods

Materials and reagents

Iron (III) acetylacetonate, manganese (III) acetylacetonate, 1,2-hexadecanediol, oleic acid, oleylamine, 1-ethyl-3-(3-dimethylaminopropyl)-carbodiiminde (EDC) and N-hydroxysuccinimide (NHS) were purchased from Macklin Biochemical Technology Co., Ltd. (Shanghai, China). DSPE-PEG-NH_2 (purity 95%) was obtained from Aladdin Chemical Company (Shanghai, China). Curcumin (Cur, purity > 99%) was purchased from Shanghai Winherb Medical S&T Development Co., Ltd. (Shanghai, China). Vascular cell adhesion molecule 1 (VCAM-1) was purchased from Apeptide Bio-Technology Co., Ltd. (Shanghai, China). The fluorescent dye Cy5.5 N-hydroxysuccinimide ester (NHS) was purchased from Shanghai Jinpan Bio-Technology Co., Ltd. (Shanghai, China). DMEM and FBS were purchased from Thermo Fisher Scientific (Waltham, MA, USA). Trypsin-EDTA (0.25%), streptomycin and penicillin were purchased from Thermo Fisher Scientific. Cell Counting Kit 8 (CCK8) was purchased from Kaiji Biological Technology Development Co., Ltd. (Nanjing, China). Fetal bovine serum (FBS) and DMEM/F12 cell culture mediums were purchased from Gibco. Unless otherwise noted, all other reagents were of analytical grade.

Preparation of the super-paramagnetic Fe_3O_4 nanoparticles (SPIO)

Superparamagnetic nanoparticles (SPION) were prepared by the high-temperature solid-state method as previously described [33]. Briefly, iron (III) acetylacetonate (2 mmol), manganese (III) acetylacetonate (2 mmol), 1,2-hexadecanediol (10 mmol), oleic acid (3 mmol) and oleylamine (3 mmol) were dissolved in 10 mL of benzyl ether in a reaction flask using a magnetic stirrer at 200°C for 2 h under argon. Following this, the reaction mixture was further heated to reflux (~300°C), stirred for 2 h. After cooling to room temperature, anhydrous ethanol (40 mL) was added and centrifuged (8000 rpm, 10 min) to obtain the brown-black complex. Precipitate was extracted and added into 10 mL of hexane, following add 0.05 mL oleic acid and 0.05 mL oleamide to remove undissolved impurities by centrifugation (8000 rpm,

10 min). Finally, the final product was collected by centrifugation at 8,000 rpm for 10 min, washed three times with absolute ethanol, and further dispersed in n-hexane.

Synthesis of compounds

Preparation of SDP and SDP/Cur nanoparticles: The SPIO@DSPE-PEG (SDP) nanoparticles were prepared with slight variations according to the method described [34]. SPIO NPs (10 mg, iron content) dissolved in 1 mL of tetrahydrofuran (THF) was mixed with DSPE-PEG-NH_2 (30 mg) dissolved in THF at room temperature for 15 min. Then, 20 mL ultrapure water was slowly and sequentially dropped into the mixed solutions under vigorous stirring, and performed with ultrasonication for 30 min. The obtained solution was dialyzed for 24 h in the distilled water with a dialysis bag (cut-off molecular weight, 3,500 Da). The dialysis solution was centrifuged (8000 rpm, 10 min) to remove small amount of undissolved materials, the resulting supernatant was collected and stored at 4°C. The whole preparation processes of SPIO@DSPE-PEG/Cur (SDP/Cur) nanoparticles were same as SDP except added 10 mg SDP and 5 mg Curcumin.

Preparation of SDP-VCAM-1/Cur nanoparticles: VCAM-1 (3 mg, 0.003 mmol) was dissolved in MES buffer (1 mL, 0.1 M). The caboxyl groups of VCAM-1 were activated with EDC solution (1.2 mg, 1 mg/mL) in MES buffer for 1 h to adjust its pH to 7.2, followed by the addition of the NHS solution (1 mg/mL, 25 μL) in PBS under stirring for 30 min to form active esters. Further, SDP/Cur (8 mg, 0.003 mmol) in PBS was added and stirring at room temperature for 4 h. The obtained solution was dialyzed for 4 h in the distilled water with a dialysis bag (cut-off molecular weight, 2,000 Da), lyophilized, and stored at 4°C.

Preparation of SDP-VCAM-1/Cur/Cy5.5 nanoparticles: SDP (30 mg) and Cy5.5-NHS (400 μL, 1 mg/mL) were added and the reaction was carried out for 12 h stored under light protection. The obtained solution was dialyzed for 24 h in the distilled water with a dialysis bag (cut-off molecular weight, 2,000 Da), lyophilized, and stored at 4°C.

Characterization of nanoparticles: The SPIO nanoparticles and compounds were determined by Fourier transforms infrared (FTIR, Tensor-27, Bruker, Germany). Samples were mixed with KBr (1:50), recorded in the range of 600-4000 cm^{-1}. The morphology and structure of the nanoparticles were performed using transmission electron microscopy (TEM, JEM-2010F, JEOL, Japan). Hydrodynamic diameters of the nanoparticles were characterized by dynamic light scattering (DLS) using a Malvern Zetasizer (Nano ZS 90, Malvern, UK). The nanoparticles were analyzed using a mass spectrometer (AB Sciex 500R, Darmstadt, Germany) to confirm the successful modification of VCAM-1 onto nanocarrier. MR tests using SDP-VCAM-1/Cur/Cy5.5 nanoparticles were characterized by evaluating the efficacy of the probe as a T_2-weighted MR imaging contrast agent. The lyophilized SPIO coated on a glass grid containing silicon substrate was exposed to X-ray Diffraction Analysis (XRD) measurements. XRD patterns of the samples were carried out in an X-ray diffraction (XRD, Rigaku D/MAX-2550, Tokyo, Japan) using Cu Kα radiation. Scan parameters: tube voltage, 40 kV; tube current, 100 mA; scanning range, 20° to 80° and scan rate of 7° min^{-1}. The magnetic property of the SPION and SDP nanoparticles was characterized by Vibrating sample magnetometer (VSM, Model 7410, Lake Shore Cryotronics, Westerville, OH, USA) at room temperature. Scan parameters: 300 Kv, N_2 environment and a magnetic field range of 2000 to -20000 kOe. The weight loss of the nanoparticles was measured by Thermal gravimetric analysis (TGA) analysis (Netzsch TG 209 F3 Tarsus, Selb, Germany) in nitrogen flow. Approximately 4-16 mg samples were sealed in open ceramic and heated from 25 to 600°C at a heating rate of 10°C/min under nitrogen atmosphere. The fluorescent signals of nanoparticles were detected by a spectrofluorometer (678 nm excitation, 694 nm emission; Shimadzu RF530PC, Kyoto, Japan).

In vitro release profile of curcumin

Encapsulation efficiency (EE%) and drug-loading efficiency (DL%) of curcumin in SDP/Cur were determined. Firstly, a calibration curve was set with Cur at concentrations of 1.25, 1.56, 2.50, 3.12, 6.25, 10.00, 12.50, 20.00, 25.00, 40.00 μg/mL analyzed using a UV-Vis spectrophotometer (Shimadzu UV-3100PC, Kyoto, Japan) in the wavenumber range 300-

600 nm. The percentage of EE and DL were calculated according to the following formula:

EE (%) = (weight of the drug in nanoparticles)/(weight of initially added drug) × 100%.

DL (%) = (weight of the drug in nanoparticles)/(weight of the nanoparticles) × 100%.

The drug release study of nanoparticles was conducted using a dialysis bag method described by Xie et al. [35]. Briefly, SDP/Cur nanoparticles (20 mg) were placed in a dialysis bag (cut-off molecular weight, 3500 Da) and the tube was rotated in 200 mL of PBS solution at pH = 7.4 at 37°C. At the prescribed time points, 1 mL of the buffer solution was taken to analyze and replaced with the amount of the fresh PBS. The concentration of the released Cur was directly determined by UV-Vis spectrophotometer with the calibration curve of Cur. The cumulative amount of Cur in SPIO@DSPE-PEG/Cur nanoparticles was calculated according to the formula:

Cumulative amount released (%) = (weight of drug released)/(weight of drug in nanoparticles) × 100%.

Biocompatibility evaluation

Mouse peritoneal macrophages (RAW264.7) cells were cultivated for *in vitro* experimental studies. RAW264.7 cells was cultured in DMEM medium supplemented with 10% F12, 100 units/mL penicillin and 100 mg/mL streptomycin in 25 cm^2 cell culture flasks. All these cells were cultured in 5% carbon dioxide at 37°C. Cells were seeded on 24-well plates at 5 × 10^4 cells per well and cultured until reaching confluence. Then, RAW264.7 cells were incubated in DMEM mediums containing SDP/Cy5.5, SDP/Cur/Cy5.5 and SDP-VCAM-1/Cur/Cy5.5 nanoparticles. At the prescribed time points, the medium was removed and 100 μl of fresh medium supplemented with 10 μl of CCK-8 solution was then added into each well. After incubation 2 h at 37°C, the absorbance (optical density, OD) was measured at a wavelength of 450 nm on a microplate reader (SH1000, Corona, Japan). The cell viability was calculated according to the formula:

$$\text{Cell viability} = \frac{A_s - A_b}{A_n - A_b} \times 100\%$$

where A_s, A_n, and A_b are the absorbance of the sample, negative control and blank group, respectively. control and blank group, respectively.

Hemolysis test

Blood was collected from SD rat and transferred to sodium citrate anticoagulant tubes at a 1:9 ratio. Then, red blood cells (RBC) were separated from plasma, and then were suspended in PBS to prepare a 16% (v/v) red blood cell suspension. Then the solution was mixed with 5 mL containing different concentrations of SDP, SDP/Cur/Cy5.5 and SDP-VCAM-1/Cur/Cy5.5 at 37°C for 6 h, then centrifuged (1000 rpm, 5 min) to sediment the red blood cell. Finally, the absorbance of supernatants was measured at a wavelength of 540 nm on a microplate reader. RBC which incubated with pure water and PBS were used as positive control and negative control, respectively. Hemolysis was calculated according to the formula:

$$\text{Cell viability} = \frac{A_s - A_n}{A_p - A_n} \times 100\%$$

where A_s, A_n and A_p are the absorbance of the sample, the negative control, and positive controls, respectively.

Coagulation studies

Prothrombin Time (PT) and Activated Partial Thromboplastin Time (APTT) are basic tests to record the time taken for the activation of blood clotting. Briefly, blood samples were collected and immediately centrifuged (3000 rpm, 20 min) to obtain the serum. At the prescribed time points, 5 mL of serum was allowed to mix with sample solution, then incubated at 30°C for 10 min. Finally, the PT or APTT reagents (100 μL) were added, and APTT and PT values of the samples were determined full-automatic blood coagulation analyzer (Sysmex Corporation, Kobe, Japan).

Cellular uptake of nanoparticles

RAW264.7 cells were cultured in confocal cell dishes at a density of 2 × 10^5 cells per well until they became completely adherent. Then the culture medium was exchanged by fresh medium, and the cells were treated with SDP/Cy5.5 and SDP-VCAM-1/Cy5.5 nanoparticles. Follow-

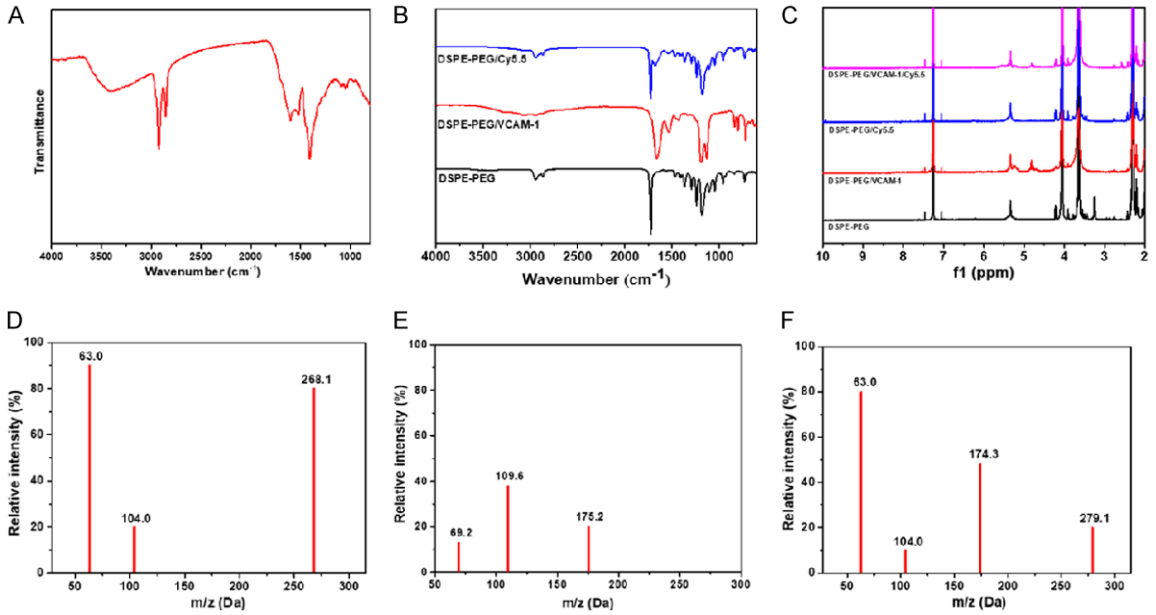

Figure 1. Characterization of nanoparticles. (A) FTIR spectra of SPIO. (B) FTIR spectra of DSPE-PEG, DSPE-PEG-VCAM-1 and DSPE-PEG/Cy5.5. (C) ^{1}H NMR spectra of DSPE-PEG, DSPE-PEG/VCAM-1, DSPE-PEG/Cy5.5 and DSPE-PEG/VCAM-1/Cy5.5 in D_2O. MS spectra of SDP (D), VCAM-1 (E) and SDP/VCAM-1 (F).

ing incubation for 4 h and 12 h, the cultured cells were washed with PBS for 3 times and fixed with 4% paraformaldehyde for 20 min. Then, cells were washed twice using PBS, followed nucleus staining with DAPI for 15 min. Intracellular localization was observed by confocal laser scanning microscopy.

Statistical analysis

All the data were presented as mean ± standard deviation (SD), and the statistical comparisons between groups were analyzed via one-way ANOVA statistical analysis by GraphPad Prism 7 software. The values of * ($P < 0.05$), ** ($P < 0.01$), and *** ($P < 0.001$) were determined to be statistically significant.

Results and discussion

Synthesis and characterization

Scheme 1 shows a schematic diagram of the preparation of Cy5.5 labeled and VCAM-1 targeted DSPE-PEG and magnetic nanoparticles loaded with curcumin micelles (SDP-VCAM-1/Cur/Cy5.5). Firstly, Superparamagnetic iron oxide nanoparticles (SPIO) was prepared by the high-temperature solid-state method and then loaded into amphiphilic polymer DSPE-PEG by hydrogen bonding in oil phase. Secondly, curcumin (Cur) was assembled on SDP micelles by self-assembly method. Through the amidation reaction between the carboxyl groups on VCAM-1 peptide and the amino groups on SDP using EDC and NHS, the VCAM-1 loaded magnetic nanomicelles (SDP-VCAM-1/Cur) were obtained. Finally, the SDP-VCAM-1/Cur/Cy5.5 nanomicelles prepared by the covalent-coupling reaction between the amino groups on SDP/Cur-VCAM and NHS on Cy5.5 hydroxysuccinimide ester.

The FTIR spectra of SPIO nanoparticles is shown in **Figure 1A**. The two peaks at 1570 cm^{-1} may be attributed to the C = O symmetrical stretching vibration and the C = N antisymmetric stretching vibration, which is related to inorganic carboxylate. The two peaks at 2920 cm^{-1} and 2850 cm^{-1} indicate the C-H telescopic vibration in oleic acid molecules. VCAM-1 was connected to DSPE-PEG through the amidation reaction between the carboxyl of VCAM-1 and the amine of DSPE-PEG as shown in **Figure 1B**. Characteristic absorption peaks of DSPE-PEG/VCAM-1 at 1527 cm^{-1} of N-H, 1438 cm^{-1} of C-N and 1664 cm^{-1} of C = O indicated the formation of amide bond. Meanwhile, characteristic absorption peaks of DSPE-PEG/Cy5.5 at 1676 cm^{-1} of C = O indicated the for-

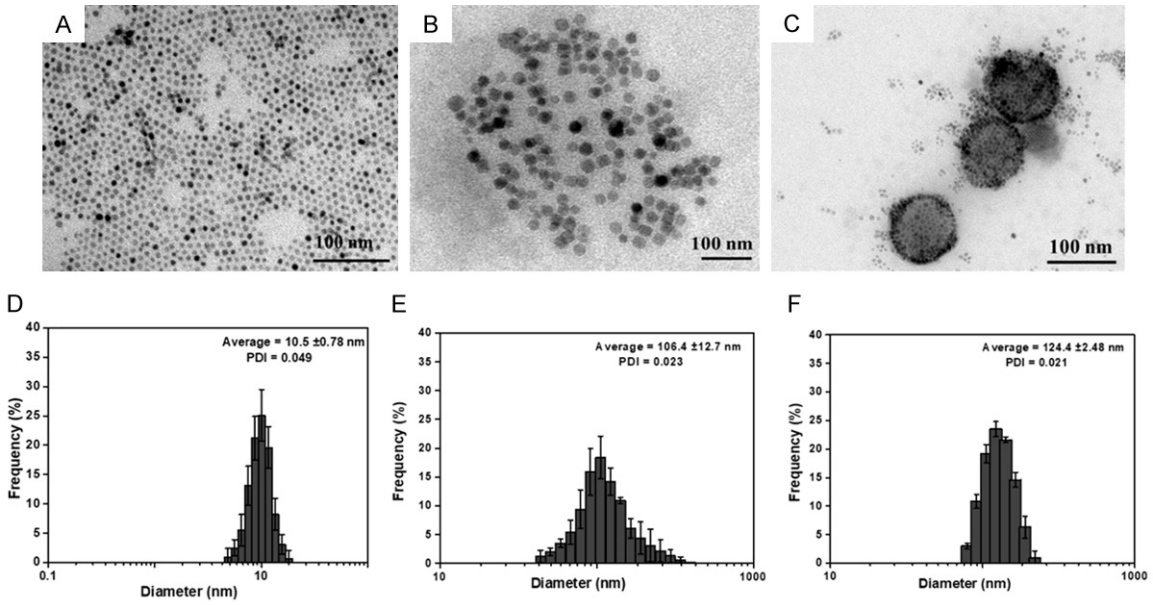

Figure 2. A. TEM images of SPIO. B. TEM images of SDP. C. TEM images of SDP/Cur. D. Particle sizes of SPIO. E. Particle sizes of SDP. F. Particle sizes of SDP/Cur.

mation of amide bond. Cy5.5 was connected to DSPE-PEG via the amidation reaction between the NHS of Cy5.5 and the amine of DSPE-PEG. As is shown in **Figure 1C**, chemical shift at 3.67 ppm presented the -CH_2- of PEG chain, and chemical shifts at 2.68 ppm was the characteristic peaks of VCAM-1. VCAM-1 and Cy5.5 were grafted to DSPE-PEG via amide reaction and characteristic ^{1}H-NMR spectra was displayed. By mass spectrometry, we confirmed that VCAM-1 is covalently conjugated to SDP nanoparticles (**Figure 1D-F**).

XRD results further confirmed that the SPIO nanoparticles were spinel-like materials (Figure S1A). It can be seen that SPIO nanoparticles exhibited obvious characteristic peaks located at: 2θ = 30.2°, 35.6°, 43.0°, 53.4°, 57.1° and 62.5°, corresponding to the (220), (311), (400), (422), (511) and (440) crystal face of inverse spinel Fe_3O_4 with a face-centered cubic phase. The chemical structure of the DSPE-PEG, DSPE-PEG/VCAM-1, DSPE-PEG/Cy5.5, DSPE-PEG/VCAM-1/Cy5.5 polymers was confirmed by FTIR and ^{1}H NMR, as presented in **Figure 1B**, **1C**.

As shown in **Figure 2A**, TEM images of SPIO exhibit a good distribution, well crystallography and clear spheres. Meanwhile, the SDP and SDP/Cur nanoparticles are spherical shape or sphere-like morphology with obvious core-shell structure, and uniformly dispersed iron oxide particles visible in the shell (**Figure 2B**, **2C**). For SPIO nanoparticles, the average particle diameter was 10.5 ± 0.78 nm (**Figure 2D**). The size measured by DLS is consistent with the hydrodynamic diameter estimated by TEM. For SDP nanoparticles, the average particle diameter was 106.4 ± 12.7 nm (**Figure 2E**). The diameter of SDP/Cur increased to 124.4 ± 2.48 nm (**Figure 2F**). These results showed that there was no significant difference in the morphology of SDP/Cur after Cur loading. A small size of nanoparticles (10-200 nm) is beneficial to enhance its ability to the tumor/inflamed regions accumulation and retention, and thus to avoid clearance by the body's defense system-the reticuloendothelial system (RES) [36]. Prior study reported that nanoparticles are easily engulfed by tumor and inflammatory cells via endocytosis, which will maximize efficacy of treatment [37].

Ultraviolet-visible and fluorescent spectrometry

Figure 3A shows the UV-vis spectra lines of DSPE-PEG and its derivatives. It can be seen that the UV absorption peak of pure Cur and Cy5.5 appear near 426.5 nm and 673.5 nm, respectively. There is no obvious characteristic absorption peak in DSPE-PEG and SDP.

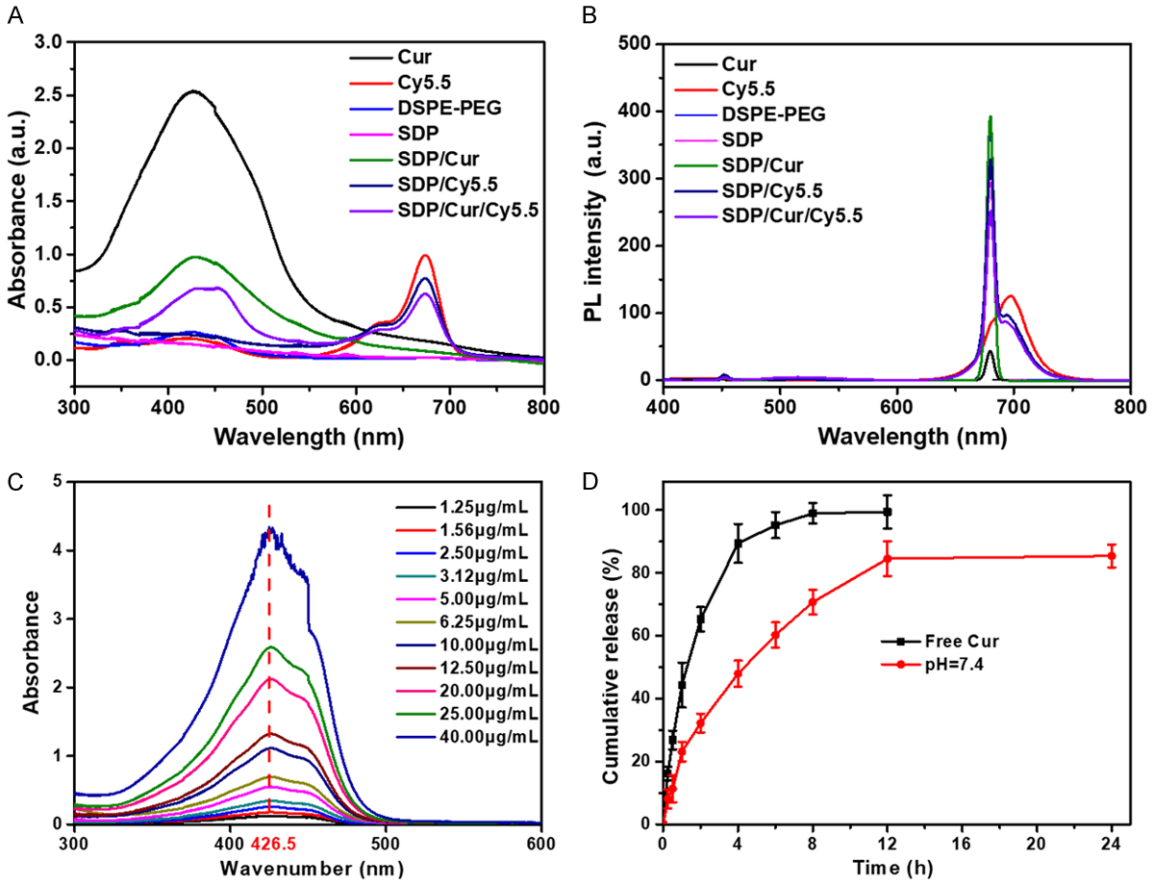

Figure 3. A. UV-vis spectra of different nanoparticles. B. PL spectra of different nanoparticles. C. UV-vis spectra of Cur at various concentrations. From this fit a wavelength of maximal absorption of ≈426.5 nm is obtained. D. Drug release profile of complexes at pH = 7.4. Data were given as the mean ± SD (n = 3).

Table 1. The encapsulation efficiency (EE%) and drug-loading efficiency (DL%)

Sample	Total mass (μg)	Added Cur mass (μg)	Measured Cur mass (μg)	Drug-loading efficiency (DL%)	Encapsulation efficiency (EE%)
SDP/CUR	100	33.3	25.6	25.6 %	76.9%
SDP-VCAM-1/CUR	100	33.3	25	25.0 %	75.1%

However, SDP/Cy5.5 and SDP/Cur/Cy5.5 nanoparticles appear a characteristic absorption peak at 673.5 nm, indicating the NPs maintained their previous optical performance after blending the SDP polymer. In addition, the intensity of UV absorption peak of SDP/Cur/Cy5.5 at the same concentration is slightly lower than pure Cy5.5, indicating that metals have a certain quenching effect on fluorescent molecules. **Figure 3B** shows the fluorescence spectra lines of DSPE-PEG and its derivatives. Comparing these two curves one can clearly find that the characteristic peaks of SDP/Cy5.5 and SDP/Cur/Cy5.5 nanoparticles at 690 nm are consistent with pure Cy5.5.

In vitro release study

The UV full wavelength scanning of Cur with different concentration was shown in **Figure 3C**, and Cur standard curves are shown in Figure S1B. As shown in **Table 1**, encapsulation efficiency (EE%) and drug-loading efficiency (DL%) of Cur in SDP/Cur nanoparticles were 76.9% and 25.6%, respectively. After modification with VCAM-1 peptide, EE% and DL% of Cur in SDP-VCAM-1/Cur nanoparticles reached 75.1%, and 25.0%, respectively. The cumulative percentages of Cur release in SDP-VCAM-1/Cur nanoparticles were evaluated in PBS (pH 7.4) compared to free CUR, as shown in **Figure**

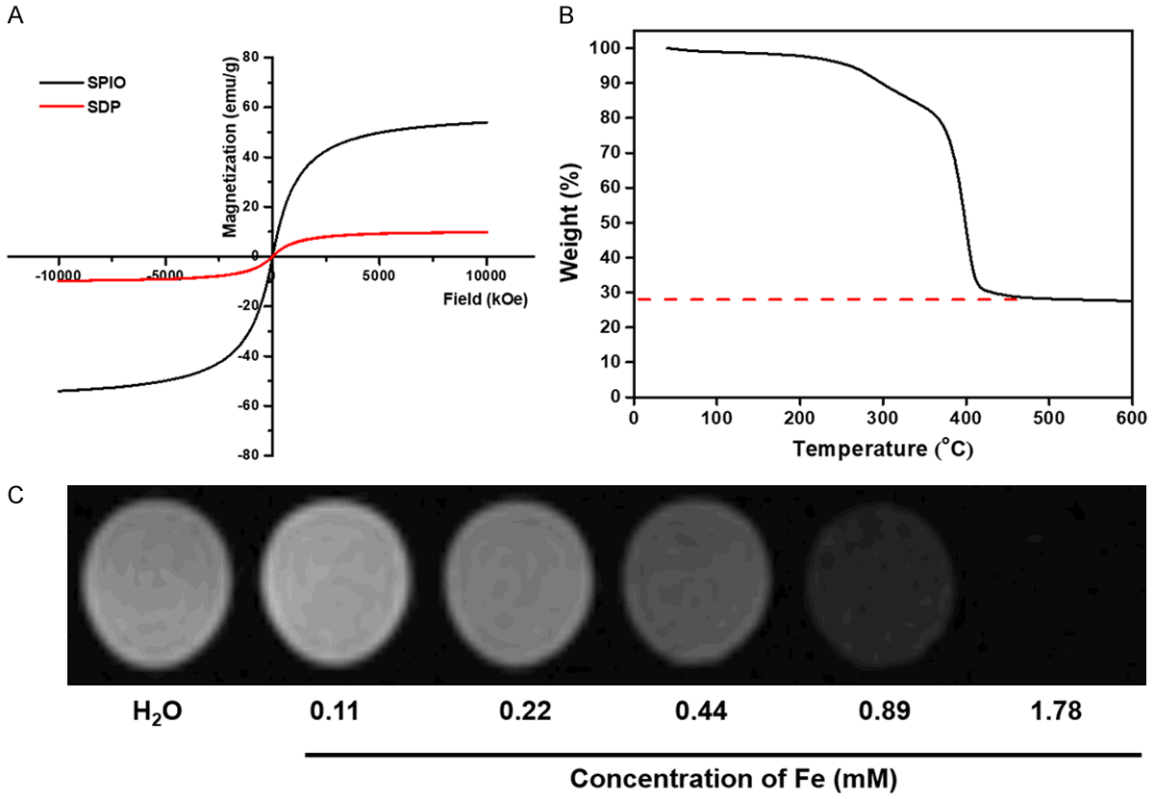

Figure 4. A. VSM of SPIO and SDP. B. TG curves of SDP. C. MR images analysis of SDP at different iron concentration.

3D. The free Cur exhibited a "release burst" within the initial 4 hours and had a cumulative release percentage of 68%. The Cur in SDP-VCAM-1/Cur nanoparticles displayed a relatively more rapid release and is followed by a relative slow release. About 32% of the Cur from these NPs was released during first 4 hours, and about 80% over the 24-hour period. The faster cumulative Cur release at the early stage was caused by the hydrophobic Cur molecules adsorbed on the outer surface of the SDP nanoparticles. Afterward, the rate of drug release declined, nearly 20% of Cur were unreleased in SDP nanoparticles even after 24 h. The sustained release of Cur was due to larger amounts of assembled Cur (hydrophobic molecules) being encapsulated in DSPE-PEG.

VSM

Magnetic response is one of the important characteristic parameters to test magnetic materials [38]. Meanwhile, the hysteresis loops reflect the ability of magnetic materials to respond to an external magnetic field. As shown in **Figure 4A**, the magnetic hysteresis curves of all samples basically pass through the origin, indicating that the hysteresis loop were close to zero and have the superparamagnetic behavior. The saturation magnetization was found to be 56 emu/g for SPIO, which proves that the monodisperse SPIO have high saturation magnetization. The saturation magnetic strength of SDP decreases to 10 emu/g, which is due to the polymer coating. However, it still reserved superparamagnetic response to the external magnetic field and can be used for following magnetic resonance imaging.

Thermogravimetric analysis

The content of SPIO in SDP nanoparticles was analyzed by thermogravimetric analysis. As shown in **Figure 4B**, the weight loss of 70% in the temperature range of 150°C to 500°C was corresponded to high temperature decomposition of DSPE-PEG. The remaining mass of SDP nanoparticles after 600°C belongs to SPIO, thus it can be calculated that the entrapment efficacy of SPIO in SDP-VCAM-1/Cy5.5 nanoparticles is 28%. Therefore, the SPIO concentrations of SDP nanoparticles were

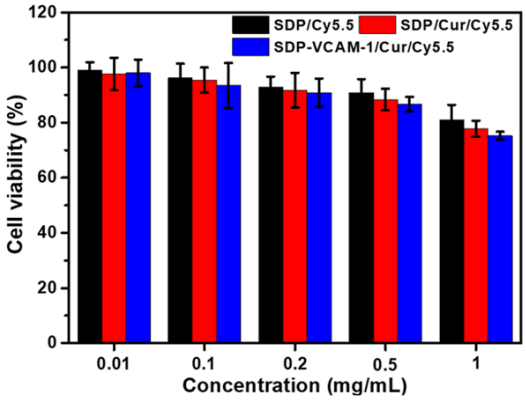

Figure 5. RAW264.7 cells viability after incubation with SDP/Cy5.5, SDP/Cur/Cy5.5 and SDP-VCAM-1/Cur/Cy5.5 at various concentrations (0.01-1 mg/mL) for 24 h by CCK-8 assay. Data were given as mean ± SD (n = 3).

more than adequate, which could be used as a perfect contrast agent for imaging and diagnosis. These results were consistent with the previous VSM results.

Magnetic resonance imaging of NPs

To assess the contrast enhancement of the SPIO nanoparticles, five different concentrations of Fe were used: (0.11 mM, 0.22 mM, 0.44 mM, 0.89 mM and 1.78 mM). As shown in **Figure 4C**, the imaging effect increased gradually as a function of added SPIO concentration. When the concentration is above 0.44 mM, it still has a good imaging effect. When the concentration is lower than 0.44 mM, the imaging effect is not suitable for complex clinical imaging. Meanwhile, MR signal ($1/T_2$*) exhibited a linear upward tendency (Figure S1C). In addition, it can be found that the R2 relaxation rate was calculated to be 64.7 $mM^{-1}S^{-1}$, indicating that the modified SPIO still retained the original crystal structures [39]. These results indicated that SDP has potential clinical application value as a CT imaging contrast agent.

Cytotoxicity of nanoparticles

The cytotoxicity of nanoparticles is an important index influencing the application of biological research, so the cytotoxicity of the nanoparticles was evaluated in Mouse macrophage cell line (RAW264.7) using the CCK8 assay. The viability of macrophage cell after incubation with SDP/Cy5.5, SDP/Cur/Cy5.5 and SDP-VCAM-1/Cur/Cy5.5 nanoparticles at varying concentrations was shown in **Figure 5**. No significant difference in cell viability was observed at various concentrations. When the concentration of nanoparticles was lower than 0.5 mg/mL, over 90% of cell viability was maintained, which satisfying the toxicity requirements as a contrast agent, providing a good guarantee for further biological experimental designs. Thus, the prepared nanoparticles did not induce obvious cytotoxicity, and showed excellent biocompatibility *in vitro*.

Blood compatibility assay

To evaluate whether the prepared nanoparticles were suitable for intravenous administration, the hemolytic test was conducted using mouse red blood cell hemolysis test *in vitro*. As shown in **Figure 6A**, the hemolysis ratio increased with the increase of the concentration of NPs. Furthermore, the hemolysis rate of SDP-VCAM-1/Cur/Cy5.5 was slightly higher compared with SDP/Cy5.5. In addition, hemolysis rate of SDP-VCAM-1/Cur/Cy5.5 nanoparticles was 7.5% at the concentration of 0.5 μg/mL. According to previous reports in the literature, the hemolysis rate of materials was higher than 5%, which will cause hemolysis to red blood cells (RBCs) [40]. This result indicates that NPs ranging from 0.1 to 0.5 mg/μL had a minor effect on the RBCs, showing the good hemocompatibility.

APTT was used to assess endogenous coagulation pathway and PT was used to evaluate exogenous coagulation pathway, which are important index of material hemocompatibility evaluation. The effect of NPs on the coagulation times and blood PLT level (APPT and PT) are presented in **Figure 6B**. There was not a significant difference in APTT and PT in SDP-VCAM-1/Cur/Cy5.5 compared with PBS at concentrations below 0.5 mg/μL. As reported in the literature, the normal ranges for APPT and PT were 11-14 s and 27-40 s [41]. Our results showed the SDP-VCAM-1/Cur/Cy5.5 at concentrations < 0.5 mg/μL did not induce intrinsic coagulation pathway and extrinsic coagulation pathway, exhibiting satisfactory hemocompatibility.

Cellular uptake tests

To verify the targeting of nanoparticles in biological applications, the cellular uptake behavior of nanoparticles by RAW264.7 cell over 12 h

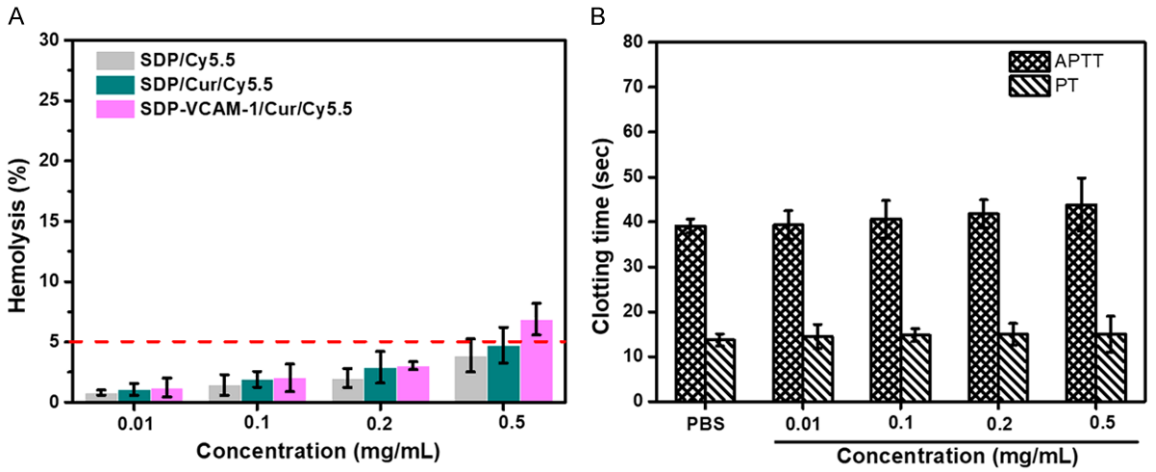

Figure 6. A. Effect of SDP/Cy5.5, SDP/Cur/Cy5.5 and SDP/Cur/Cy5.5 with different concentrations on hemolysis. Biomaterials are classified as non and slightly hemolytic (0-5% hemolysis), or hemolytic (> 5% hemolysis). B. Effect of SDP-VCAM-1/Cur/Cy5.5 on APTT and PT with PBS as control. The normal ranges for APPT and PT were 11-14 s and 27-40 s.

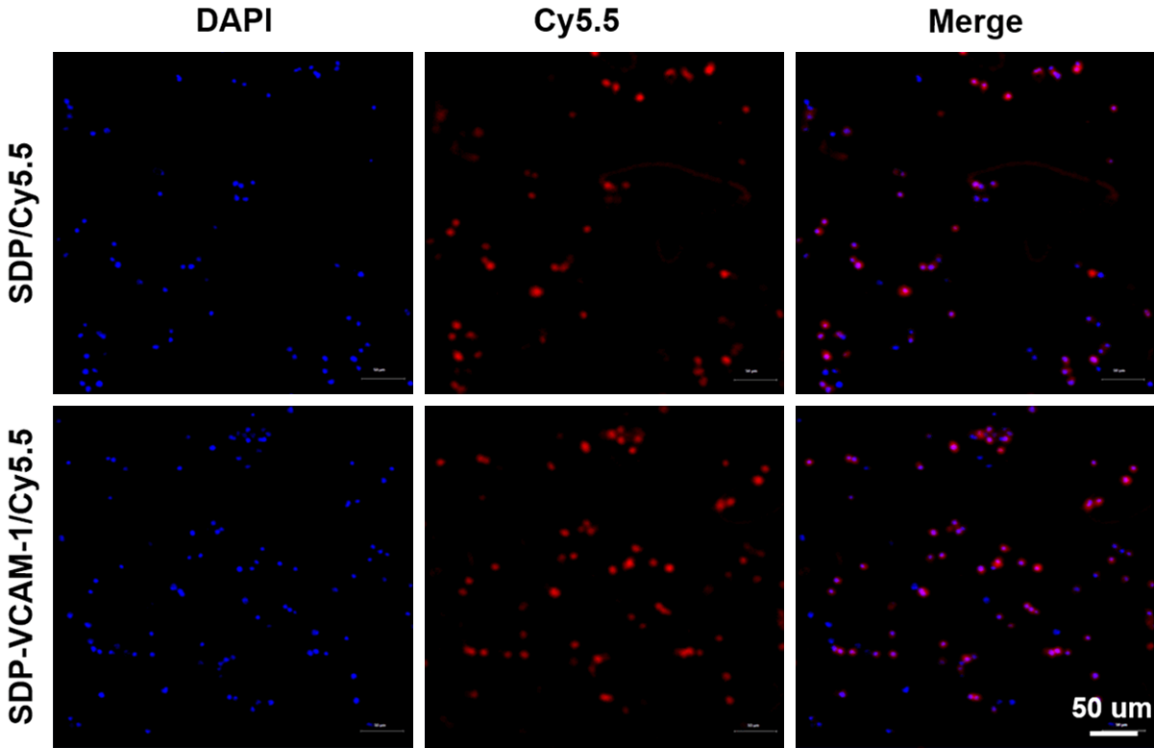

Figure 7. Confocal images of the cellular uptake induced by SDP/Cy5.5 and SDP-VCAM-1/Cur/Cy5.5 in RAW264.7 cells. The NPs gave red fluorescent and the nucleus gave blue fluorescence.

time period was monitored by the Confocal laser scanning microscopy (CLSM). As shown in **Figure 7**, the nuclei were stained with DAPI (blue), and the red fluorescent nanoparticles gather in the nuclear area. It is clear from CLSM image that the SDP/Cy5.5 nanoparticles have a small amount of fluorescence at excitation wavelength 678 nm, while the SDP-VCAM-1/Cur/Cy5.5 nanoparticles have a large amount of fluorescence, which confirm the effectiveness of the VCAM-1 target molecules. All results showed that the prepared SDP-VCAM-1/Cur/

Cy5.5 nanoparticles have certain targeting ability *in vitro* and can be selectively taken up by macrophages.

Conclusions

Multifunctional SDP-VCAM-1/Cur/Cy5.5 nanoparticles were successfully constructed by conjugation of Cy5.5 and VCAM-1 into the DSPE-PEG coated SPIO and Cur for MR/fluorescence dual-modal imaging and chemotherapy of glioma. All prepared nanoparticles were characterized by their FT-IR, ^{1}H-NMR spectra and mass spectral data, which confirmed the successfully loading of Cy5.5 and VCAM into the SDP nanoparticles. The TEM images and DLS dates confirmed the nanoparticles were uniform size and good dispersion with an obvious core-shell structure. The fluorescence spectra confirmed nanoparticles exhibited better stability and higher fluorescent intensity. The obtained nanoparticles showed super para-magnetism and presented good MRI imaging efficiency. The nanoparticles exhibited a sustained release of drugs compared with free curcumin. The CCK-8 assay confirmed that the nanoparticles have no effect on cell cytotoxicity and indicate the biocompatibility, which would be suitable for biomedical applications. Furthermore, the confocal imaging data confirmed efficient targeting of the nanoparticles to the macrophages. Meanwhile, the prepared nanoparticles at concentrations < ~0.5 mg/μL exhibited good hemocompatibility, with a hemolysis rate less than 5%. Our results demonstrate that the prepared multifunctional nanoparticles are appropriate for use in pathological event in atherosclerosis, which provide a novel therapeutic way for atherosclerosis.

Disclosure of conflict of interest

None.

Address correspondence to: Dr. Yunhong Xu, Department of Cardiology, The Third Affiliated Hospital of Guangzhou Medical University, No. 63, Duobao Road, Liwan District, Guangzhou 510150, Guangdong, P. R. China. Tel: +86-13697479017; E-mail: sharonxyh123@126.com

References

[1] Jeon S, Kim T, Jeong S, Jung I, Kim N, Lee M, Sonn S, Seo S, Jin J, Kweon H, Kim S, Shim D, Park Y, Lee S, Kim K, Cybulsky M, Shim H, Roh T, Park W, Lee H, Choi J, Park S and Oh GJ. Anti-Inflammatory actions of soluble ninjurin-1 ameliorate atherosclerosis. Circulation 2020; 142: 1736-1751.

[2] Tyrrell D and Goldstein DJ. Ageing and atherosclerosis: vascular intrinsic and extrinsic factors and potential role of IL-6. Nat Rev Cardiol 2020; 18: 58-68.

[3] Kumar D, Narang R, Sreenivas V, Rastogi V, Bhatia J, Saluja D and Srivastava K. Circulatory miR-133b and miR-21 as novel biomarkers in early prediction and diagnosis of coronary artery disease. Genes 2020; 11: 164.

[4] Goel S, Guo L, Liu B and Kent KJ. Mechanisms of post-intervention arterial remodelling. Eur Heart J 2012; 96: 363-371.

[5] Nicol P, Lutter C, Bulin A, Castellanos MI, Lenz T, Hoppmann P, Lahmann AL, Colleran R, Euller K, Steigerwald K, Neubauer S, Rechenmacher F, Ludwig BS, Weinmuller M, Kerch G, Guo L, Cheng Q, Acampado E, Koppara T, Kessler H and Joner M. Assessment of a pro-healing stent in an animal model of early neoatherosclerosis. Sci Rep 2020; 10: 8227.

[6] Lu B, Han X, Zhao A, Luo D, Maitz MF, Wang H, Yang P and Huang N. Intelligent H2S release coating for regulating vascular remodeling. Bioact Mater 2021; 6: 1040-1050.

[7] Gallo D, Bijari PB, Morbiducci U, Qiao Y, Xie YJ, Etesami M, Habets D, Lakatta EG, Wasserman BA and Steinman DA. Segment-specific associations between local haemodynamic and imaging markers of early atherosclerosis at the carotid artery: an in vivo human study. J R Soc Interface 2018; 15: 20180352.

[8] Patil R, Galstyan A, Grodzinski ZB, Shatalova ES, Wagner S, Israel LL, Ding H, Black KL, Ljubimova JY and Holler E. Single- and multi-arm gadolinium MRI contrast agents for targeted imaging of glioblastoma. Int J Nanomedicine 2020; 15: 3057-3070.

[9] Norouzi M, Yathindranath V, Thliveris JA and Miller DW. Salinomycin-loaded iron oxide nanoparticles for glioblastoma therapy. Nanomaterials (Basel) 2020; 10: 477.

[10] Lu ZR, Mohs AM, Zong Y and Feng Y. Polydisulfide Gd(III) chelates as biodegradable macromolecular magnetic resonance imaging contrast agents. Int J Nanomedicine 2006; 1: 31-40.

[11] Zheng S, Zhang M, Bai H, He M, Dong L, Cai L, Zhao M, Wang Q, Xu K and Li J. Preparation of AS1411 aptamer modified Mn-MoS(2) QDs for targeted MR imaging and fluorescence labelling of renal cell carcinoma. Int J Nanomedicine 2019; 14: 9513-9524.

[12] Fan X, Yuan Z, Shou C, Fan G, Wang H, Gao F, Rui Y, Xu K and Yin P. cRGD-conjugated Fe(3)

O(4)@PDA-DOX multifunctional nanocomposites for MRI and antitumor chemo-photothermal therapy. Int J Nanomedicine 2019; 14: 9631-9645.

[13] Kim HM, Kim DM, Jeong C, Park SY, Cha MG, Ha Y, Jang D, Kyeong S, Pham XH, Hahm E, Lee SH, Jeong DH, Lee YS, Kim DE and Jun BH. Assembly of plasmonic and magnetic nanoparticles with fluorescent silica shell layer for trifunctional SERS-magnetic-fluorescence probes and its bioapplications. Sci Rep 2018; 8: 13938-13938.

[14] Ashokan A, Somasundaram VH, Gowd GS, Anna IM, Malarvizhi GL, Sridharan B, Jobanputra RB, Peethambaran R, Unni AKK, Nair S and Koyakutty M. Biomineral nano-theranostic agent for magnetic resonance image guided, augmented radiofrequency ablation of liver tumor. Sci Rep 2017; 7: 14481-14481.

[15] Luo R, Zhou X, Chen Y, Tuo S, Jiang F, Niu X, Pan F and Wang H. Lysozyme aptamer-functionalized magnetic nanoparticles for the purification of lysozyme from chicken egg white. Foods 2019; 8: 67.

[16] Ning J, Wang M, Luo X, Hu Q, Hou R, Chen W, Chen D, Wang J and Liu J. SiO(2) stabilized magnetic nanoparticles as a highly effective catalyst for the degradation of basic fuchsin in industrial dye wastewaters. Molecules 2018; 23: 2573.

[17] Babu K and Dhamodharan R. Synthesis of polymer grafted magnetite nanoparticle with the highest grafting density via controlled radical polymerization. Nanoscale Res Lett 2009; 4: 1090-1102.

[18] Mondal S, Manivasagan P, Bharathiraja S, Santha Moorthy M, Nguyen VT, Kim HH, Nam SY, Lee KD and Oh J. Hydroxyapatite coated iron oxide nanoparticles: a promising nanomaterial for magnetic hyperthermia cancer treatment. Nanomaterials (Basel) 2017; 7: 426.

[19] Li L, Wu C, Pan L, Li X, Kuang A, Cai H and Tian R. Bombesin-functionalized superparamagnetic iron oxide nanoparticles for dual-modality MR/NIRFI in mouse models of breast cancer. Int J Nanomedicine 2019; 14: 6721-6732.

[20] Zhang N, Cai X, Gao W, Wang R, Xu C, Yao Y, Hao L, Sheng D, Chen H, Wang Z and Zheng Y. A multifunctional theranostic nanoagent for dual-mode image-guided HIFU/chemo- synergistic cancer therapy. Theranostics 2016; 6: 404-417.

[21] Nakamura M, Hayashi K, Kubo H, Harada M, Izumi K, Tsuruo Y and Yogo T. Mesoscopic multimodal imaging provides new insight to tumor tissue evaluation: an example of macrophage imaging of hepatic tumor using organosilica nanoparticles. Sci Rep 2017; 7: 3953.

[22] O'Farrell N, Houlton A and Horrocks BR. Silicon nanoparticles: applications in cell biology and medicine. Int J Nanomedicine 2006; 1: 451-472.

[23] Wycisk V, Achazi K, Hirsch O, Kuehne C, Dernedde J, Haag R and Licha K. Heterobifunctional dyes: highly fluorescent linkers based on cyanine dyes. ChemistryOpen 2017; 6: 437-446.

[24] Hekman MC, Rijpkema M, Muselaers CH, Oosterwijk E, Hulsbergen-Van de Kaa CA, Boerman OC, Oyen WJ, Langenhuijsen JF and Mulders PF. Tumor-targeted dual-modality imaging to improve intraoperative visualization of clear cell renal cell carcinoma: a first in man study. Theranostics 2018; 8: 2161-2170.

[25] Vanden-Hehir S, Tipping WJ, Lee M, Brunton VG, Williams A and Hulme AN. Raman imaging of nanocarriers for drug delivery. Nanomaterials (Basel) 2019; 9: 341.

[26] Gogineni V, Maddirela D, Park W, Jagtap J, Parchur A, Sharma G, Ibrahim E, Joshi A, Larson A, Kim D and White S. Localized and triggered release of oxaliplatin for the treatment of colorectal liver metastasis. J Cancer 2020; 11: 6982-6991.

[27] Zhang E, Zhukova V, Semyonkin A, Osipova N, Malinovskaya Y, Maksimenko O, Chernikov V, Sokolov M, Grigartzik L, Sabel B, Gelperina S and Henrich-Noack P. Release kinetics of fluorescent dyes from PLGA nanoparticles in retinal blood vessels: in vivo monitoring and ex vivo localization. Eur J Pharm Biopharm 2020; 150: 131-142.

[28] Patel SK and Janjic JM. Macrophage targeted theranostics as personalized nanomedicine strategies for inflammatory diseases. Theranostics 2015; 5: 150-172.

[29] Mlinar L, Chung E, Wonder E and Tirrell M. Active targeting of early and mid-stage atherosclerotic plaques using self-assembled peptide amphiphile micelles. Biomaterials 2014; 35: 8678-8686.

[30] Libby P. Inflammation in atherosclerosis. Nature 2002; 420: 868-874.

[31] Cybulsky M, Iiyama K, Li H, Zhu SN, Chen M, Iiyama M, Davis V, Gutierrez-Ramos JC, Connelly P and Milstone D. A major role for VCAM-1, but not ICAM-1, in early atherosclerosis. J Clin Invest 2001; 107: 1255-1262.

[32] Dimastromatteo J, Broisat A, Perret P, Ahmadi M, Boturyn D, Dumy P, Fagret D, Riou LM and Ghezzi C. In vivo molecular imaging of atherosclerotic lesions in ApoE-/- mice using VCAM-1-specific, 99mTc-labeled peptidic sequences. J Nucl Med 2013; 54: 1442.

[33] Li WJ, Wang Y, Liu Y, Wu T, Cai WL, Shuai XT and Hong GB. Preliminary study of MR and fluorescence dual-mode imaging: combined

macrophage-targeted and superparamagnetic polymeric micelles. Int J Med Sci 2018; 15: 129-141.

[34] Li L, Wu C, Pan L, Li X, Kuang A, Cai H and Tian R. Bombesin-functionalized superparamagnetic iron oxide nanoparticles for dual-modality MR/NIRFI in mouse models of breast cancer. Int J Nanomedicine 2019; 14: 6721-6732.

[35] Xie X, Wang H, Williams GR, Yang Y, Zheng Y, Wu J and Zhu LM. Erythrocyte membrane cloaked curcumin-loaded nanoparticles for enhanced chemotherapy. Pharmaceutics 2019; 11: 429.

[36] Zaloga J, Janko C, Nowak J, Matuszak J, Knaup S, Eberbeck D, Tietze R, Unterweger H, Friedrich RP, Duerr S, Heimke-Brinck R, Baum E, Cicha I, Dörje F, Odenbach S, Lyer S, Lee G and Alexiou C. Development of a lauric acid/albumin hybrid iron oxide nanoparticle system with improved biocompatibility. Int J Nanomedicine 2014; 9: 4847-4866.

[37] Im GB, Kim YH, Kim YJ, Kim SW, Jung E, Jeong GJ, Wang K, Kim J, Kim DI, Kim TH, Yi GR, Yu T and Bhang SH. Enhancing the wound healing effect of conditioned medium collected from mesenchymal stem cells with high passage number using bioreducible nanoparticles. Int J Mol Sci 2019; 20: 4835.

[38] Lin WC, Chuang CC, Chang CJ, Chiu YH and Tang CM. The effect of electrode topography on the magnetic properties and mri application of electrochemically-deposited, synthesized, cobalt-substituted hydroxyapatite. Nanomaterials (Basel) 2019; 9: 200.

[39] Fang Y, Lin S, Yang F, Situ J, Lin S and Luo Y. Aptamer-conjugated multifunctional polymeric nanoparticles as cancer-targeted, MRI-ultrasensitive drug delivery systems for treatment of castration-resistant prostate cancer. Biomed Res Int 2020; 2020: 9186583.

[40] Song B, Yang L, Han L and Jia L. Metal ion-chelated tannic acid coating for hemostatic dressing. Materials (Basel) 2019; 12: 1803.

[41] Liang C, Li N, Cai Z, Liang R, Zheng X, Deng L, Feng L, Guo R and Wei B. Co-encapsulation of magnetic FeO nanoparticles and doxorubicin into biocompatible PLGA-PEG nanocarriers for early detection and treatment of tumours. Artif Cells Nanomed Biotechnol 2019; 47: 4211-4221.

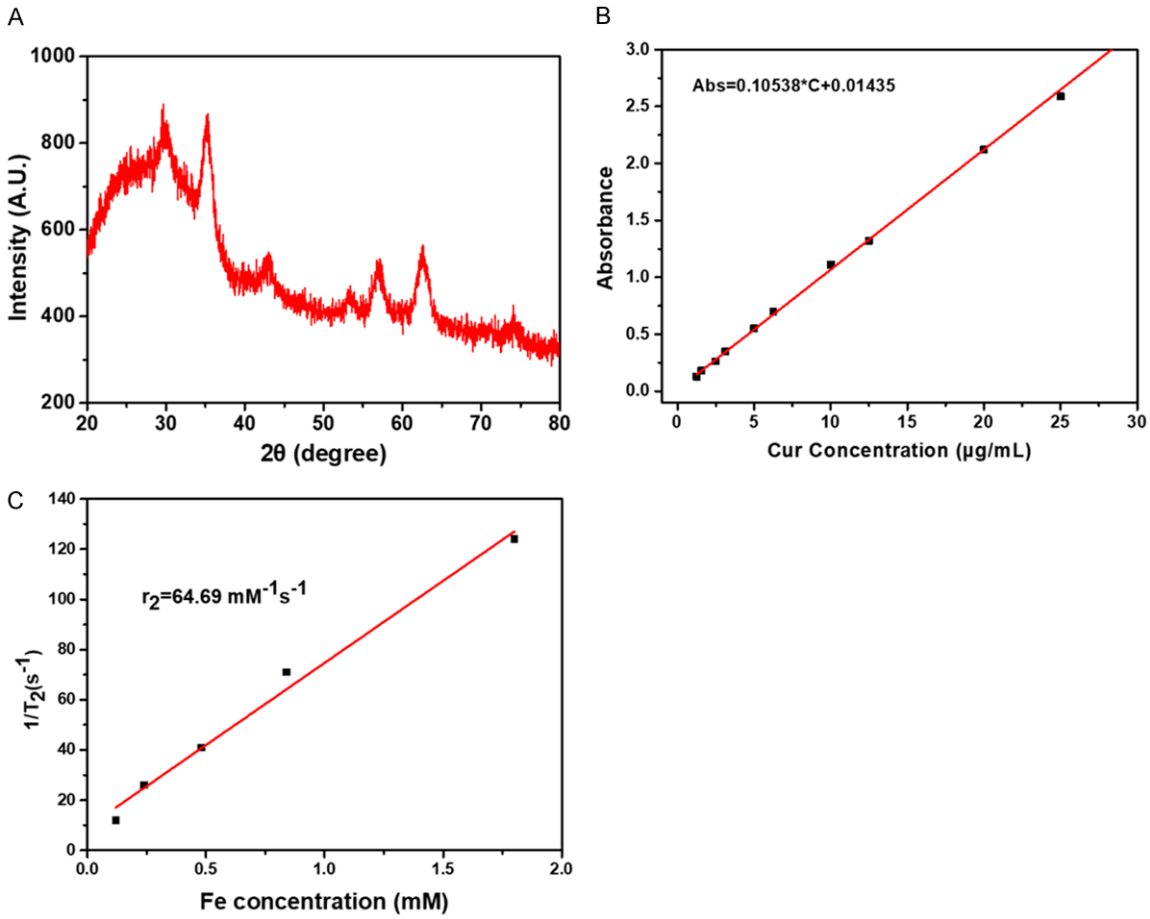

Figure S1. A. XRD of SPIO. B. The standard curve of Cur. C. T_2 relaxation rate ($1/T_2$) against Fe concentrations of SDP.